Systematic Controller Design for Inverter-based Microgrids with Certified Large-Signal Stability and Domain of Attraction

Buxin She, *Student Member, IEEE,* Jianzhe Liu, *Member, IEEE,* Feng Qiu, *Senior Member, IEEE,* Hantao Cui, *Senior Member, IEEE,* Nattapat Praisuwanna, *Student Member, IEEE,* Jingxin Wang, *Member, IEEE,* Leon M. Tolbert, *Fellow, IEEE,* Fangxing Li, *Fellow, IEEE*

***Abstract*—Inverter-based resources (IBRs) introduce fast dynamics and high non-linearities to microgrids, degrading their stability and complicating the design of effective controllers. To address the arising vulnerability and non-linearities, this paper presents a systematic controller design approach that ensures large-signal stability and domain of attraction (DOA) for islanded microgrids. First, the nonlinear electromagnetic transient model of inverter-based microgrids is developed in the rotating *dq* reference frame, which is then transformed to a homogeneous-like system with nonlinear terms acting as superimposed parameter uncertainties. Next, the stability conditions, including certified stability, certified DOA, and their combination, are derived to rigorously guarantee a designated range to be a subset of DOA. The designated region is customized and flexible enough to cover microgrids' normal or emergency operational ranges, such as low- and high-voltage ride-through (L/HVRT) conditions. Then, a systematic method for identifying the candidate control parameter set is developed by integrating the analytical stability conditions. This approach is further exemplified in the droop controller design to improve microgrid stability and resilience. Finally, the proposed systematic controller design is verified through numerical simulation and power hardware-in-the-loop experiments to ensure large-signal stability and DOA of microgrids in emergency L/HVRT conditions.**

***Index Terms*—Islanded microgrid, electromagnetic transient model, inverter-based resources, large-signal stability, domain of attraction.**

I. Introduction

THE need to transform the energy system away from its reliance on fossil fuels to renewable energy resources is driving the rapid development of microgrids. A microgrid can function like a generation source in grid-connected mode or operate as an insolated, self-sufficient system in islanded mode [1]. Islanded microgrids are gaining more attention due to their flexibility and capability to accommodate renewable energy resources, supply critical loads locally, and improve power system resilience after extreme events [2].

Stability is one of the essential factors in optimizing microgrid operation or designing microgrid controllers [3]. However, the high penetration of inverter-based resources (IBRs) can degrade the stability of microgrids and pose challenges to the existing operation and control framework [4]. On the one hand, the dynamics of IBRs are much faster than those of synchronous generators, thereby posing greater threats to the stability of microgrids [3]. On the other hand, IBRs are expected to be more actively involved in grid service, i.e., switching between grid-following (GFL) mode and grid-forming (GFM) mode, and providing auxiliary service by adaptively changing control parameters [5]. This further necessitates a more rigorous guarantee of stability.

Research on the stability of ac microgrids is mainly categorized into local stability (small-signal stability) and transient stability (large-signal stability) [6]. Small-signal stability analysis focuses on a sufficiently small region around an equilibrium, which can be represented by various linearized models such as the state space model [7], [8], transfer function model [9], and impedance model [10]. The relevant analytical criteria, i.e., eigenvalue [11], root locus [9], Middlebrook's stability criterion [12], and Nyquist criteria [13], can be used for small-signal stability estimation and integrated into dynamic controller design [14] or economic operation [15].

A stable equilibrium induces a region where each trajectory starts and eventually converges to the equilibrium itself, referred to as the domain of attraction (DOA). Small-signal stability criteria, which typically rely on a linearized model, generally cannot explicitly characterize the geometry of the DOA. However, this information is critical in determining the stability condition of ac microgrids when they deviate significantly from equilibrium after a large disturbance [16]. Hence, the large-signal stability of ac microgrids has been the subject of research.

Like small-signal stability, several criteria have been developed for determining the large-signal stability of nonlinear ac microgrids, based on Lyapunov's direct method [17], Popov's absolute method [18], bifurcation theory [16], singular perturbation theory [19], and equal area method [20]. These criteria can be used for DOA estimation. For example, Ref. [17] estimated the DOA of islanded microgrids by enlarging the candidate state set until the Lyapunov stability condition is

B. She, F. Li, N. Praisuwanna, J. Wang, L.M. Tolbert are with the Dept. of EECS, The University of Tennessee, Knoxville, TN, USA. Emails: bshe@vols.utk.edu, fli6@utk.edu, npraisu1@vols.utk.edu, jwang78@utk.edu, and tolbert@utk.edu

J. Liu is with the Energy Systems and Infrastructure Analysis Division, Argonne National Laboratory, Lemont, IL 60439, USA, and the Consortium for Advanced Science and Engineering, The University of Chicago, Chicago, IL 60637, USA. Email: jianzhe.liu@ieee.org.

F. Qiu is with the Energy Systems and Infrastructure Analysis Division, Argonne National Laboratory, Lemont, IL 60439, USA. Email: fqiu@anl.gov.

H. Cui is with the School of ECE, Oklahoma State Univ., Stillwater, OK, USA.

F. Li and J. Liu are co-corresponding authors.

infeasible. Ref. [21] estimated the DOA of a droop-controlled inverter connected to an infinite bus using Takagi-Sugeno multi-modeling. In [22], the converter is simplified as an ideal current source controlled by a phase-locked loop (PLL). Then, periodical DOA is obtained by transforming the certified Lyapunov stability condition into semidefinite programming (SDP) and solving it with the sum-of-squares programming (SOS) method. Except for DOA estimation, these criteria have been applied in controller design to certify transient stability. Ref. [19] derived the sufficient frequency stability conditions for controllers using a simplified system model that omits network topology and voltage dynamics. The maximum active power perturbation, the system damping, and the frequency are bounded to a specific range so that there exists a positive definite Lyapunov function that can guarantee stability. In [23], the large-signal stability boundaries are derived to guarantee the transient performance of GFL and GFM inverters. Ref. [24] ensures the transient stability of droop-controlled inverter networks when subject to multiple operating constraints based on a physically meaningful Lyapunov-like function and derived mathematical and computational stability criteria. Ref. [25] designed various topology change strategies for inverter-based microgrids while guaranteeing large-signal stability using Takagi-Sugeno fuzzy modeling.

Despite extensive research into the large-signal stability of ac microgrids, existing works have some limitations that must be addressed. First, a more detailed electromagnetic transient (EMT) model is expected to be used due to the involvement of the fast dynamics of power electronic devices. A few studies use simplified inverter models without modeling voltage and current regulation loops [22], [24]–[27] or reduced network models through Kron reduction [19], [25]. Second, the detailed modeling will be used to extend the transient analysis from a single-inverter or parallel-inverter system [20], [28] to general networked-inverter microgrids. Third, although some research could estimate the DOA of nonlinear microgrids, they usually rely on the direct inspection of stability criteria without performance guarantees, i.e., guaranteeing stable operation in low- and high-voltage-ride-through (L/HVRT) conditions. Fourth, existing research on ac microgrids has derived constraints for ensuring stability with the varying of line impedance [27] but has not systematically designed the control modes or control parameters to actively modify the geometry of a DOA to contain a certain operational range. This is particularly important for actively participating in grid services, both in normal and emergency situations.

To bridge the gap in the existing literature, this paper proposes a systematic controller design approach for inverter-based microgrids to certify stability and DOA. A nonlinear EMT model of droop-controlled islanded microgrids is formulated with detailed dynamic modeling of the device-level controller and network-side behavior. This model is then transformed into a homogeneous-like system with nonlinear terms as superimposed parameter uncertainties to facilitate the analytical stability analysis. Based on the nonlinear model, the stability criteria certifying that a given set is contained in the system DOA is rigorously derived. Next, a systematic approach that integrates the analytical stability conditions is developed to identify the candidate parameter set, which can be integrated into the existing online adaptive methods [27] and inform the data-driven control [29]. The proposed approach is then exemplified in droop controller design so as to improve microgrid stability and resilience. Based on the discussion above, the contributions of this manuscript are as follows:

- Formulation of an EMT model and a homogeneous-like model of inverter-based microgrids that facilitates analytical stability analysis and controller design.
- Derivation of criteria that certify large-signal stability and a designated DOA of microgrids based on the formulated full-scaled model.
- Development of a systematic control design approach that integrates the derived stability conditions, and validation through numerical and power hardware-in-the-loop (HIL) experiments.

The rest of this paper is organized as follows. Section II introduces the EMT model of inverter-based islanded microgrids. Section III derives the analytical criteria that can certify stability and DOA, which are then integrated into the systematic controller design. The droop controller design exemplifies the systematic approach to ensure stability and DOA. In Section IV, a single inverter system and a modified Banshee microgrid are used to verify the proposed method. Finally, Section V concludes this paper and discusses future research directions.

II. Electromagnetic Transient Model of Inverter-based Microgrids

This section presents the EMT model of inverter-based microgrids in a rotating *dq* reference frame, which is then transformed into a homogeneous-like system to facilitate the analytical stability analysis.

A. Component Modeling

Fig. 1 shows the grid components of an inverter-based islanded microgrid, including GFM inverters, connection lines, buses, and loads [17]. The dynamics of each component can be described by a general model given in (1). Then, the modeling of each component may be combined to create a unified model of the microgrid.

$$\begin{cases} \dot{x}_c = A_c\left(x_c\right) x_c + B_c u_c \\ y_c = C\left(x_c\right) x_c \end{cases} \tag{1}$$

where x_c is the component state variable; y_c is the component output variable, and u_c is the component input variable. Each variable is further categorized based on the grid component it represents. For example, x_c could specifically refer to inverter states denoted as x_{inv}, load states denoted as x_r, line states denoted as x_l, or bus states denoted as x_b. Eq. (1) is a nonlinear model with the state variable embedded in the state matrix A_c.

All the grid components are modeled under the rotating reference frame. Specifically, each inverter is regulated at the local rotating dq reference frame, and one of the local references serves as the global rotating DQ reference frame for the rest of the grid components. Then, the variables observed

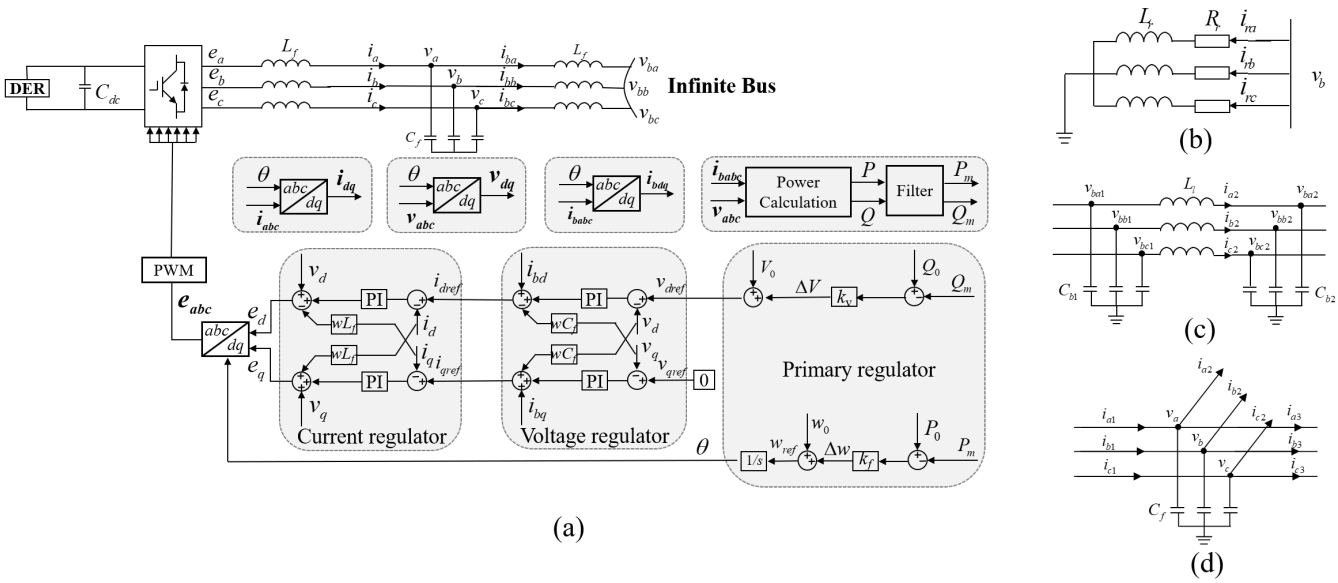

Fig. 1. Diagram of inverter-based microgrid components: (a) droop-controlled GFM inverter; (b) load; (c) line; (d) bus.

from the local dq reference frame are transferred to global DQ reference frame [25]:

$$\mathbf{x}_{cDQ} = \mathbf{T_S}\mathbf{x}_{cdq} = \begin{bmatrix} \cos\theta_i & -\sin\theta_i \\ \sin\theta_i & \cos\theta_i \end{bmatrix} \mathbf{x}_{cdq} \tag{2}$$

where $\mathbf{x}_{cDQ} = [x_{cD}(t), x_{cQ}(t)]$ and $\mathbf{x}_{cdq} = [x_{cd}(t), x_{cq}(t)]$ are the state vectors observed on the DQ/dq-axis from the global and local reference frame, respectively, and θ is the angle mismatch between the two references.

1) GMF inverter: Fig. 1(a) shows the diagram of a GFM inverter, which consists of a current regulator, a voltage regulator, and a primary regulator, each with several parameters that need elaborate design. The mathematical modeling [17], [25], [30] is detailed in (3)-(8).

- Power angle

$$\dot{\theta} = \omega_{ref} - \omega_{DQ} \tag{3}$$

- Droop equation

$$\begin{cases} v_{dref} = V_n + k_{dv}\left(Q_n - Q_m\right) \\ w_{ref} = w_n + k_{df}\left(P_n - P_m\right) \end{cases} \tag{4}$$

- Low pass filter

$$\begin{cases} P_m = \frac{G_P}{1+sT_P} P \\ Q_m = \frac{G_Q}{1+sT_Q} Q \end{cases} \tag{5}$$

- Power stage loop

$$\begin{cases} P = v_d i_{bd} + v_q i_{bq} \\ Q = v_d i_{bq} - v_q i_{bd} \end{cases} \tag{6}$$

- Current regulation loop

$$\begin{cases} i_{dref} = \left(k_{pid} + \frac{k_{iid}}{s}\right)\left(v_{dref} - v_d\right) - w_n C_f v_q + i_{bd} \\ i_{qref} = \left(k_{piq} + \frac{k_{iiq}}{s}\right)\left(v_{qref} - v_q\right) + w_n C_f v_d + i_{bq} \end{cases} \tag{7}$$

- Voltage regulation loop

$$\begin{cases} e_d = \left(k_{pvd} + \frac{k_{ivd}}{s}\right)\left(i_{dref} - i_d\right) - w_n L_f i_q + v_d \\ e_q = \left(k_{pvq} + \frac{k_{ivq}}{s}\right)\left(i_{qref} - i_q\right) + w_n L_f i_d + v_q \end{cases} \tag{8}$$

Then, a full-scaled 13*th* order state space model is obtained by introducing internal variables in (9). The nonlinear state space model has $x_{inv} = [\theta, \varphi_{vd}, \varphi_{vq}, \varphi_{id}, \varphi_{iq}, v_d, v_q, i_d, i_q, P_m, Q_m, i_{bd}, i_{bq}]^T$ as the state variable, bus voltage $u_{inv} = [v_{bD}, v_{bQ}]^T$ as the input, and filter current $y_{inv} = [i_{bD}, i_{bQ}]^T$ as the output.

$$\begin{cases} \varphi_{id} = \frac{k_{iid}}{s}\left(i_{dref} - i_d\right) \\ \varphi_{iq} = \frac{k_{iiq}}{s}\left(i_{qref} - i_q\right) \\ \varphi_{vd} = \frac{k_{ivd}}{s}\left(v_{dref} - v_d\right) \\ \varphi_{vq} = \frac{k_{ivq}}{s}\left(v_{qref} - v_q\right) \end{cases} \tag{9}$$

The full-scaled inverter model brings non-linearities to microgrids, which are reflected in (2) and (6). Eq. (2) contains the sines and cosines functions, which are further multiplied by state variables, and (6) contains the product of two state variables.

Papers [21], [25] show that reduced-order inverter modeling can cause conservatism when estimating the DOA of inverter-based systems. Utilizing the full-scaled inverter model in this paper improves modeling accuracy, thus avoiding the conservatism of analytical stability estimation resulting from model reduction. In addition, the stability of microgrids is fundamentally determined by a set of control parameters such as droop gains, proportional integral gains, and filter inductance, all of which require careful design. By grouping these parameters into a vector K, this paper focuses on designing K to ensure both large-signal stability and DOA certification.

2) Network component: The network components operate in the global rotating DQ reference frame. Figs. 1(b)-(d) show the diagram of a constant RL load, a π connection line, and a general bus. Considering that each line is connected to two independent buses, its capacitors are integrated into the connected bus to reduce the number of state variables and thus simplify the modeling. By implementing Kirchhoffs Circuit Law and performing Park Transformation, network components have distinct state variables, input variables, and output variables as follows:

(*i*). Load: $x_r = [i_{rD}, i_{rQ}]^T$, $u_r = [v_{bD}, v_{bQ}]^T$, and $y_r = [i_{rD}, i_{rQ}]^T$;

(*ii*). Line: $x_l = [i_{lD}, i_{lQ}]^T$, $u_l = [v_{bD1}, v_{bQ1}, v_{bD2}, v_{bQ2}]^T$, and $y_l = [i_{lD}, i_{lQ}]^T$;

(*iii*). Bus: $x_b = [v_{bD}, i_{bQ}]^T$, $u_b = [i_{bD1}, i_{bQ1}, i_{bD2}, i_{bQ2} \cdots]^T$, and $y_b = [v_{bD}, v_{bQ}]^T$.

The detailed expressions for each model can be found in [17], [25], [31], where the accuracy of these models has been demonstrated to be sufficient for stability analysis. Other control structures, such as distributed voltage and frequency control, can be integrated into the modeling framework and expressed in state-space form [32]. These component models, once formulated, serve as the basis for constructing a unified microgrid model that incorporates the nonlinearities of each component and the interconnections between grid components.

B. Unified Microgrid Modeling

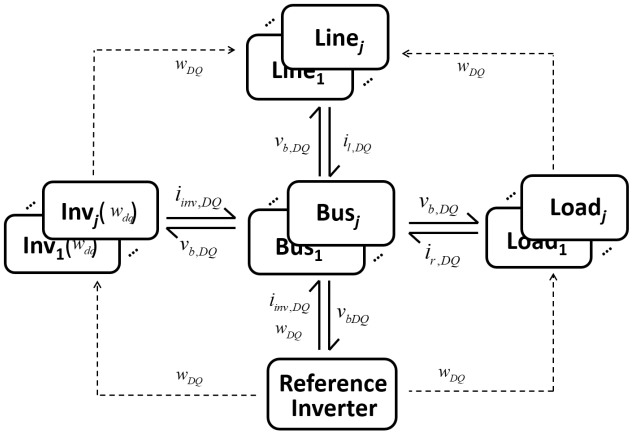

Fig. 2. Unification of microgrid components.

Assuming a reference inverter that provides the global rotating DQ reference frame for all the microgrid components, the remaining inverters are referred to as the following inverters in this paper. As visualized in Fig. 2, the unified microgrid model is formulated by coupling the grid components [17], [25]. By plugging the output of grid components into the state space model of the corresponding coupling components, the unified model is obtained in (10).

$$\dot{x} = Ax = \begin{bmatrix} A_{inv} & 0 & 0 & A_{inv-b} \\ A_{r-inv} & A_r & 0 & A_{r-b} \\ A_{l-inv} & 0 & A_l & A_{l-b} \\ A_{b-inv} & A_{b-r} & A_{b-l} & A_b \end{bmatrix} x \quad (10)$$

where A is the state matrix of the unified model, and A_{inv}, A_r, A_l, and A_b are the united state matrix of inverters, load, lines, and bus, respectively. The off-diagonal matrices represent the coupling between grid components, which matches the data flow shown in Fig. 2. The diagonal elements do not have any inner coupling, except for A_{inv}. Denote the state matrix of the reference inverter as $A_{inv,ref}$, and the following inverters are numbered from 1 to j. Then, (11) details A_{inv}.

$$A_{inv} = \begin{bmatrix} A_{inv,ref} & 0 & 0 & 0 \\ A_{inv,ref-1} & A_{inv,1} & 0 & 0 \\ \vdots & 0 & \ddots & 0 \\ A_{inv,ref-j} & 0 & 0 & A_{inv,j} \end{bmatrix} \quad (11)$$

where $A_{inv,j}$ is the state matrix of the jth following inverter and $A_{inv,ref-j}$ is the coupling between the reference inverter and the jth following inverter. The reference inverter couples with the following inverters via w_{DQ}, as visualized in Fig. 2.

In summary, component unification eliminates the input and output variables of each component modeling and makes the microgrid a unified system. Then, matrix A with embedding K can be used for analytical stability analysis and controller design.

C. Homogeneous-Like System

To better track the nonlinear dynamics of (10), it is changed into a homogeneous-like system through a coordinate transformation [33]. Assume an equilibrium x_e exists and define the state deviation from the equilibrium as $\Delta x \triangleq x - x_e$. Plug Δx and x_e into (10), then (10) is transformed into a homogeneous-like form while preserving the nonlinearities. The stability of the transformed system is the same as the original system [33], but it is more suitable for analytical stability analysis.

$$\Delta\dot{x} = \hat{A}(\Delta x, K, x_e)\Delta x = \hat{A}(h)\Delta x \quad (12)$$

where $h = h(\Delta x, K, x_e)$ is the nonlinear terms in $\hat{A}$. Note that in inverter-based microgrids, the system parameters may experience changes due to the degradation of crucial components like power switches and capacitors. These variations can impact the RLC parameters in (11), but they can also be incorporated into h for stability analysis. Then, (12) represents a homogeneous linear parameter varying (LPV) system with h as a superimposed parameter uncertainty. The stability of an LPV system could be guaranteed by bounding h to a specific range, which is fundamental to the systematic controller design in Section III.

III. Systematic Controller Design with Certified Stability and Domain of Attraction

This section derives the analytical criteria that can certify stability and DOA and integrates them into microgrid controller design.

A. Foundamentals of the systematic design

1) Concept of certified stability and DOA: DOA is a set that contains an equilibrium and lies in the state space such that each trajectory that enters it will remain inside and eventually converge to the equilibrium [20].

A microgrid is stable for sure if the system state is initialized within its DOA whether in normal or emergency conditions. IEEE standard [34] and some institution guidelines define a few important operational requirements for microgrids, i.e.,

the 1% frequency deviation limit and 7% voltage deviation limit after normal disturbances, and L/HVRT capability when there is 40% voltage deviation under emergency conditions [35]. These requirements define a critical set for microgrids, which is desired to be a subset of the DOA and can be referred to as the "designated DOA" [36]. This concept is shown in *Definition 1* and Eq. (13).

Definition 1. *A microgrid governed by* (12) *is called stable with a guaranteed DOA if $\Delta\mathcal{X}^{\mathrm{o}}$ is a subset of the system DOA.*

$$\begin{cases} \Delta\mathcal{X}^{\mathrm{o}} \triangleq \{\Delta x \in \mathbb{R}^n : \Delta x \in [\Delta\bar{x}_-, \Delta\bar{x}_+]\} \\ \Delta\mathcal{X}^{\mathrm{o}} \subset DOA \end{cases} \tag{13}$$

where $\Delta\bar{x}_-$ and $\Delta\bar{x}_+$ are the upper and lower bound of state variable deviation, which is customized and defined according to IEEE standards or institution requirements.

2) Objective of the controller design: Matrix $\hat{A}$ is composed of x_e, Δx, and K, all together fundamentally determining whether or not a microgrid meets (13). If the designated DOA contains any operation point outside the actual DOA, microgrids may encounter unexpected stability issues [36]. Hence, this paper aims to systematically design $\mathcal{K}$, the candidate set of K, such that any element of $\mathcal{K}$ makes (12) stable with a guaranteed DOA.

B. Analytical certified stability and DOA

This subsection derives the analytical conditions that certify stability, DOA, and their combination, with the assumption that K remains constant throughout.

1) Certified stability: Given the homogeneous-like system (12), there is a quadratic Lyapunov function $V(\Delta x(t)) \triangleq \Delta x(t)^\top P \Delta x(t)$ that can certify stability, where $P \succ 0$ is a positive definite matrix.

Since $\hat{A}$ is bounded internally by h, define $\mathcal{H}$ as the complete set of h that can guarantee the homogeneous-like system (12) stable. $\mathcal{H}$ is a convex hull according to [37]. Although $\mathcal{H}$ is difficult to represent explicitly, it is possible to find a subset $\mathcal{H}'$ by introducing a base vector and a scaling factor. Denote the subset as $\mathcal{H}' \triangleq \left\{h : h \in \left[\beta h_-^o, \beta h_+^o\right]\right\} \subseteq \mathcal{H}$, where h_-^o and h_+^o are guessed base vectors of the convex hull. Then, the stability condition is formulated in (14) by maximizing the scaling factor while satisfying the Lyapunov stability criteria.

$$\begin{aligned} \textbf{Certified stability:} \quad & \max_{P\succ 0, \beta>0} \beta \\ \text{s.t. } & \hat{A}^T P + P\hat{A} \leq -I, P > I \end{aligned} \tag{14}$$

Eq. (14) induces *Lemma 1*, which is then integrated into the controller design process. It determines a subset of $\mathcal{H}$ and a common quadratic Lyapunov function that renders the nonlinear system (12) Hurwitz stable.

Lemma 1. *For given $h_-^o \leq 0$ and $h_+^o > 0$, if β and P are the solution of semi-definite programming* (14)*, $V(\Delta x) = \Delta x^\top P \Delta x$ is a common quadratic Lyapunov function for* (12) *with $\dot{V}(\Delta x) < 0$ for $h \in [\beta h_-^o, \beta h_+^o]$.*

2) Certified DOA: This condition aims to find a minimum sub-level set of DOA that covers $\Delta\mathcal{X}^{\mathrm{o}}$. Assume an open set $D \subset \mathbb{R}^n$ contains the equilibrium point x_e and a continuous, differentiable Lyapunov function $V : D \to \mathbb{R}$, then (15) certified a subset of DOA and (16) further describes a positive invariant domain in a DOA [22].

$$\begin{cases} V(0) = 0 \\ V(\Delta x) > 0, \forall x \in D\backslash\{0\} \\ \dot{V}(\Delta x) = \nabla V \dot{\Delta x} \leq 0, \forall \Delta x \in D\backslash\{0\} \end{cases} \tag{15}$$

$$\mathcal{S} = \{\Delta x \in \mathbb{R}^n \mid V(\Delta x) \leq \alpha\} \quad \text{with} \quad \mathcal{S} \subset DOA \tag{16}$$

Since $P \succ 0$ and quadratic V have been obtained in (14), it is trivial to find the invariant sub-domain defined by (16): $\mathcal{S}(P,\alpha) = \left\{\Delta x : \Delta x^\top P \Delta x \leq \alpha\right\}$. Then, multi-linear matrix inequalities (LMIs) are formulated in (17) to certify $\Delta\mathcal{X}^{\mathrm{o}} \subset \mathcal{S}(P,\alpha)$, which finally ensures $\Delta\mathcal{X}^{\mathrm{o}} \subset \mathcal{S}(P,\alpha) \subset DOA$ and induces *Lemma 2*.

$$\begin{aligned} \textbf{Certifed DOA:} \quad & \min_{\alpha>0} \alpha \\ \text{s.t. } & \left(\Delta\mathcal{X}_k^{\mathrm{o}}\right)^\top P \Delta\mathcal{X}_k^{\mathrm{o}} \leq \alpha, k = 1, \cdots, m \end{aligned} \tag{17}$$

where $\Delta\mathcal{X}_k^{\mathrm{o}}$ is the k_{th} vertex of $\Delta\mathcal{X}^{\mathrm{o}}$ and m is the number of vertices.

Through the minimization of α, (17) identifies the minimum sub-level set of DOA that covers $\Delta\mathcal{X}^{\mathrm{o}}$. While this process typically involves multiple LMIs, the symmetrical property of $\Delta\mathcal{X}^{\mathrm{o}}$ can be leveraged to transform into a single LMI to reduce the computational burden. In (17), each P will certify an ellipse sub-level set of DOA, which needs to cover the expected range $\Delta\mathcal{X}^{\mathrm{o}}$. To achieve this, a minimum-volume symmetric ellipsoid covering $\Delta\mathcal{X}^{\mathrm{o}}$ can first be found, followed by the identification of a sub-level set that contains the symmetric ellipsoid. Remarkably, each of these steps requires only a single LMI [38], significantly improving computational efficiency.

Lemma 2. *For given $\beta > 0$ and $P \succ 0$ as the solution of* (14) *and α as the solution of* (17)*, $\mathcal{S}(P,\alpha) = \left\{\Delta x : \Delta x^\top P \Delta x \leq \alpha\right\}$ is the minimum ellipsoid set that covers $\Delta\mathcal{X}_k^{\mathrm{o}}$.*

3) Combined stability and DOA: The stability condition in (14) and the certified DOA (17) could be combined as a unified condition in (18) with the following logic:

- Eq. (18–1) guarantees $\Delta\mathcal{X}^{\mathrm{o}} \subset \mathcal{S}(\gamma,1)$, where $\mathcal{S}(\gamma,1) \triangleq \left\{\Delta x : \Delta x^\top [\gamma] \Delta x \leq 1\right\}$;
- Eq. (18–2) guarantees $\mathcal{S}(\gamma,1) \subset \mathcal{S}(P,1)$;
- Eq. (18–3) combined with constraint $P \succ 0$ is like (14), rendering the nonlinear system (12) Hurwitz stable.

$$\begin{aligned} \textbf{Co-Stability-DOA:} \quad & \max_{P\succ 0, \gamma>0} \det \mathrm{rootn}(P) \\ \text{s.t. } & \begin{cases} \left(\Delta\mathcal{X}_k^{\mathrm{o}}\right)^\top [\gamma] \Delta\mathcal{X}_k^{\mathrm{o}} \leq 1 & (18-1) \\ P \preceq [\gamma] & (18-2) \\ \hat{A}^T P + P\hat{A} \prec 0 & (18-3) \end{cases} \end{aligned} \tag{18}$$

Then, (18) minimizes the volume of $\mathcal{S}(P,1)$ and certifies stability and DOA as $\Delta\mathcal{X}^{\mathrm{o}} \subset \mathcal{S}(\gamma,1) \subset \mathcal{S}(P,1) \subset DOA$. Fig. 3 visualized the set-covering relationship, which further

induces *Lemma 3*. Note that β is a decision variable in (18), which can be found through the line-search method to make (18) and the set-covering feasible.

Lemma 3. *For given $\beta > 0$, $\gamma \succ 0$ and $P \succ 0$ as the solution of* (18)*, $\mathcal{S}(\gamma, 1) = \{\Delta x : \Delta x^\top P \Delta x \leq \alpha\}$ is the minimum symmetric ellipsoid set that covers $\mathcal{X}_k^o$, which is also the subset of DOA .*

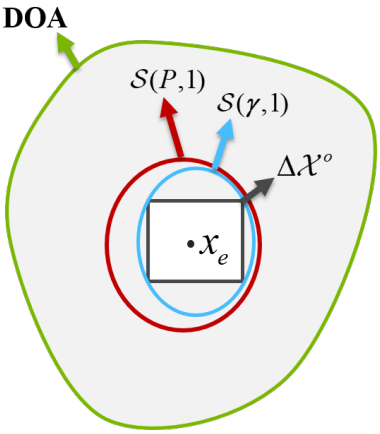

Fig. 3. Visualized set-covering relationship.

C. Systematic controller design

1) Mathematical formulation: Sub-section III-B derives the analytical condition that makes (13) feasible, assuming K as constant parameters. The systematic design changes K to decision variables and embeds the derived stability condition, as formulated in (19).

$$\textbf{Candidate-set:} \quad \mathcal{K}$$
$$\text{s.t.} \begin{cases} P \succ 0, \beta > 0, \alpha > 0, \gamma > 0 \\ (14),(17) \text{ or } (18) \end{cases} \tag{19}$$

Where $\mathcal{K}$ is the set of K subject to the constraints in (19).

Either the separate stability conditions (14) and (17), or the combined stability (18), can be included in the systematic design. For the separate conditions, K first impacts the range of the superimposed parameter uncertainty h that makes (14) feasible and then determines whether or not (17) is feasible to have an ellipsoid set covering $\mathcal{X}^{\text{o}}$. For the combined condition, K directly impact P solved by (18-3) since K is included in $\hat{A}$, which further determines whether or not $\mathcal{S}(P, 1)$ (red ellipse in Fig. 3) has a sub-set $\mathcal{S}(\gamma, 1)$ (blue ellipse in Fig. 3) to cover $\mathcal{X}^{\text{o}}$. Hence, (19) groups the inner coupling between control parameter, equilibrium, and state deviations and defines a candidate parameter set that certifies stability and designated DOA, which further induces *Lemma 4*.

Lemma 4. *If $\mathcal{K}$ defined by* (19) *isn't an empty set, any $K \in \mathcal{K}$ ensures stability with a certified DOA for system* (10)*.*

Note the proposed method is applicable to transmission or other dynamic systems represented by ordinary differential equations. New parameters can be seamlessly incorporated vector K for systematic design and stability guarantee.

2) Practical design: Although (19) rigorously defines a candidate set that certified stability and DOA, it is challenging to find the exact set or derive the explicit expressions for $\mathcal{K}$. This also makes analytical sensitivity analysis difficult. As a result, a practical design approach is further proposed to find a sub-set of $\mathcal{K}$.

Assume a base vector K_0 and a scaling factor λ. Through a line-search method, it is trivial to find a subset $\mathcal{K}' \triangleq \lambda K_0$ where $\lambda \in [\lambda_-, \lambda_+]$, and λ_- and λ_+ are the minimum and maximum λ making (19) feasible. The detailed progress is shown in *Algorithm 1*.

Algorithm 1 Identify candidate parameter set to make system (10) stable with a guaranteed DOA

Input: state space matrices: $\hat{A}$; constraints set: $\mathcal{X}^e$; target parameter vector: K, designated DOA: $\Delta\mathcal{X}^{\text{o}}$; initial guess: h_-^o, h_+^o, β, K_0, and λ_0; and searching interval $\Delta\lambda$.
Output: Candidate control parameter set: $\mathcal{K}'$.
Step 1: Identify upper boundary of $\mathcal{K}'$.
Assume $K = (1 + k\Delta\lambda)K_0$; obtain subset $\mathcal{H}'$ and the minimum subset of DOA by solving (18); increase k to k_{up} until (18) is infeasible; then, $\lambda_+ = 1 + k_{up}\Delta\lambda$.
Step 2: Identify lower boundary of $\mathcal{K}'$.
Assume $K = (1 - k\Delta\lambda)K_0$; obtain subset $\mathcal{H}'$ and the minimum subset of DOA by solving (18); decrease k to k_{down} until (18) is infeasible; then, $\lambda_- = 1 - k_{down}\Delta\lambda$.
Step 3: Obtain $\mathcal{K}'$.
$\mathcal{K}' \leftarrow \{K \in \mathbb{R}^n \mid K = \lambda K_0, \lambda_- \leq \lambda \leq \lambda_+\}$.

Note that it is unnecessary to include all control parameters in K, but rather to choose any combination of target parameters with less confidence. Furthermore, such a design is flexible since the designated DOA can be customized to include the normal and emergency operational ranges, such as L/HVRT requirements.

The practical design does not directly formulate the control law for microgrids. Instead, it takes a systematic approach to determine the subset of secure candidate control parameters. By utilizing the feasible candidate set obtained, it is convenient to incorporate it into any controller design, including adaptive control, optimal control, or data-driven control that involves online parameter updates. This method allows for the systematic design of microgrid controllers to ensure stability with a designated DOA, which is particularly crucial for power grids that are penetrated by IBRs or DERs and at risk of instability. In addition, simulation-based sensitivity analysis can be conducted by introducing uncertainties to critical parameters. In the following, the practical design is exemplified by droop-controlled GFM inverters.

D. Exemplify in droop controller design

A droop controller for IBRs is designed to emulate the behavior of conventional synchronous generators and automatically share the load among generations. Due to its rapid response and crucial power-sharing functionality, the droop gain tuning results fundamentally determine the microgrid's stability [39].

Eq. (20) represents a candidate set of droop gains for microgrid GMF inverters to ensure stability and DOA. Then, *Algorithm 1* can be utilized to obtain a subset $\mathcal{K}'$ bounded by λ_- and λ_+.

$$\textbf{Candidate-droop-gain:} \quad \mathcal{K}$$
$$\text{s.t.} \begin{cases} P \succ 0, \beta > 0, \alpha > 0, \gamma > 0 \\ K = \lambda[k_{dv,1}, k_{df,1}, \cdots, k_{dv,i}, k_{df,i}, \cdots] \\ (14),(17) \text{ or } (18) \end{cases} \tag{20}$$

Where $k_{dv,i}$ and $k_{df,i}$ are the voltage droop gain and frequency droop gain of the ith inverter, respectively.

IV. Case Studies

This section demonstrates the proposed method in a single inverter system and a modified real-world microgrid. The numerical simulation environment is equipped with an Intel(R) Core i7-8665U CPU running at 2.10 GHz, 16 GB of memory, and a MATLAB R2020a simulation platform. *Algorithm 1* is executed using CVX and MOSEK, while the dynamic performance of microgrids with the systematic design is verified using the MATLAB ode45 solver.

A. Single-inverter system

1) Systematic droop controller design: Assume a single droop-controlled GFM inverter connected to an infinite bus, as shown in Fig. 1, and find the candidate droop gain set that can certify stability and DOA under L/HVRT conditions with the proposed systematic approach. Table. I shows the key parameters of the single-inverter system.

TABLE I. Parameters of single-inverter system

Item	Value	Item	value	Item	Value
L_{f1} (p.u.)	5.25×10^{-6}	k_{dv0}	0.05	k_{df0}	0.01
C_f (p.u.)	1.9×10^{-4}	kp_{vd}	0.05	ki_{vd}	0.5
L_{f2} (p.u.)	5.25×10^{-4}	kp_{vq}	0.05	ki_{vq}	0.5
T_{fP}	0.004	kp_{id}	0.5	ki_{id}	5
T_{fQ}	0.004	kp_{iq}	0.5	ki_{iq}	5

According to IEEE Standard 1547-2018 [40], IBRs must be able to ride through short-duration voltage disturbances. The required voltage for L/HVRT is not a fixed value and depends on the specific requirements of the power system and the technical capabilities of the IBRs. This paper chooses 40% voltage deviation (v_b droops as low as 0.6 p.u. and increases as high as 1.4 p.u.) as the L/HVRT operational boundary.

Then, Fig. (4) visualizes the systematic design results with the implementation of *Algorithm 1*, where λ_- and λ_+ are solved as 0.036 and 1.828, respectively. Then, the candidate droop gain set is obtained as $\mathcal{K}' = \{K \in \mathbb{R}^2 \mid K = \lambda[k_{dv0}, k_{df0}], 0.036 \leq \lambda \leq 1.828\}$. Based on *Lemma 4*, for $\forall [k_{dv}, k_{df}] \in \mathcal{K}'$, the single inverter system is stable with guaranteed DOA covering L/HVRT operational range.

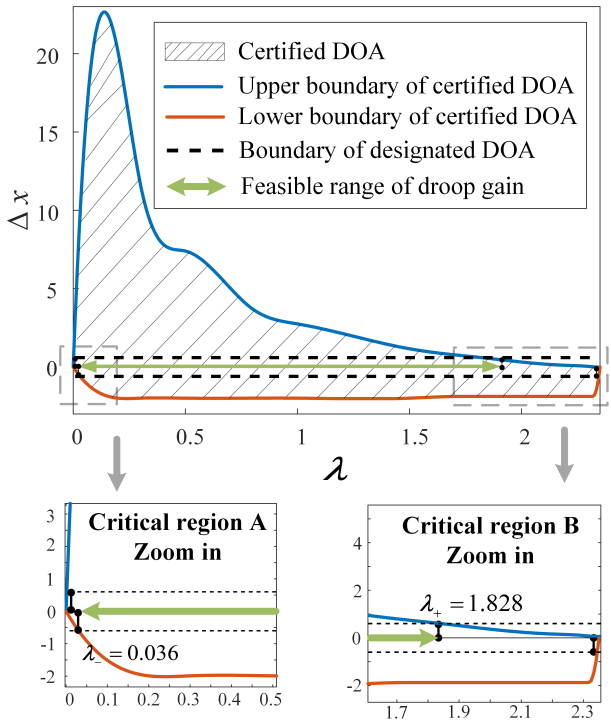

Fig. 4. Visualized systematic droop controller design results for single inverter system.

2) Numerical Verification: To ensure design correctness, randomly sample droop gains from set $\mathcal{K}'$. They are tested through time domain simulation (TDS) in Matlab using an ode45 solver with a relative tolerance of 5×10^{-6} and an absolute tolerance of 5×10^{-5}. The control performance is assessed by perturbing the state variables from equilibrium and observing their transient trajectories. This is a common way to evaluate the performance of the state space model in the control theory and power system [41], [42].

TDS results show that all state variables converge to equilibrium with randomly sampled droop gains in $\mathcal{K}'$. For instance, Fig. 5a shows the transient trajectories of the single-inverter system when initialized from the L/HVRT boundary with $\lambda = 1 \in \mathcal{K}'$ and $[k_{dv}, k_{df}] = [0.0525, 0.015]$. The system stabilizes with all state variables converging to equilibrium at around 0.15 seconds. Conversely, if $\lambda = 2.5 \notin \mathcal{K}'$ and $[k_{dv}, k_{df}] = [0.125, 0.025]$, the system is demonstrated to diverge when initialized from the L/HVRT boundary, and the corresponding transient trajectories are displayed in Fig. 5b.

3) Comparison: This paper proposes a new controller design approach that utilizes a full-scaled homogeneous-like EMT model. It ensures stability and designated DOA flexibly. A comparison study is conducted to highlight the advantages of this approach. The comparison involves implementing the proposed systematic approach in controller design using a simplified IBR model [21]. The study also tries a DOA estimation method [22] for controller design but finds the estimated DOA may fail to cover the L/HVRT range as desired.

Using a simplified IBR model and *Algorithm 1*, λ_- and λ_+ are solved as 0.50 and 1.78 in Fig. 6, respectively. Then, the candidate droop gain set yields $\mathcal{K}' =$

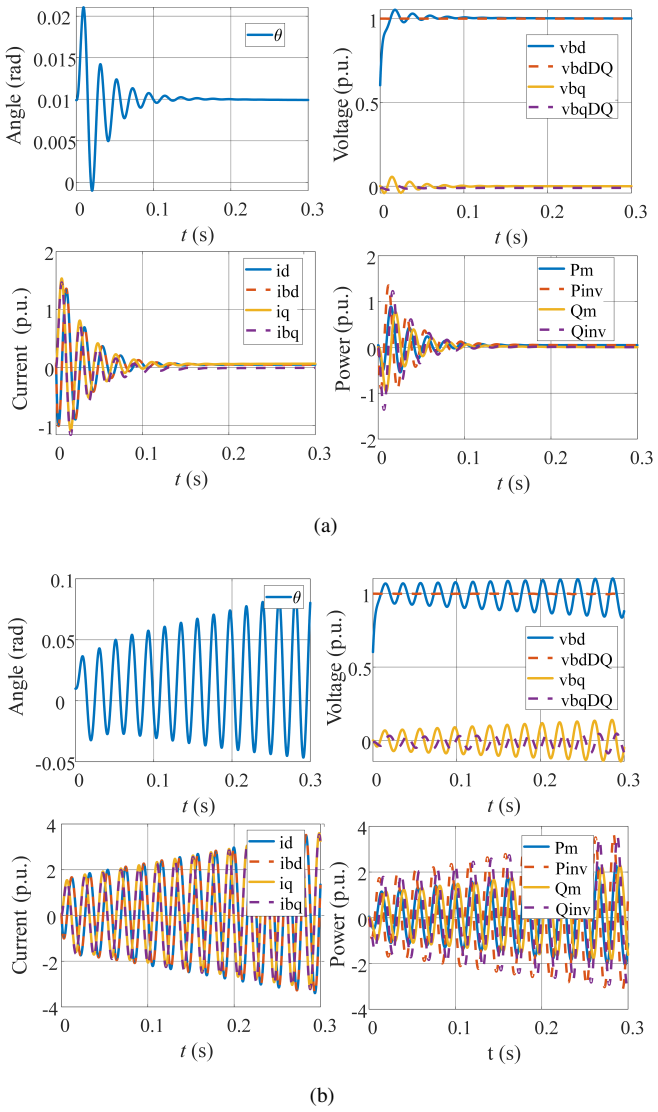

Fig. 5. Transient trajectories of single-inverter system: (a) $[k_{dv}, k_{df}] = [0.0525, 0.015]$, (b) $[k_{dv}, k_{df}] = [0.125, 0.025]$.

$\{K \in \mathbb{R}^2 \mid K = \lambda[k_{dv0}, k_{df0}], 0.50 \leq \lambda \leq 1.78\}$, which is smaller than the set obtained based on full-scale model. Such conservativeness resulting from model reduction aligns with the observations in [21].

If solely relying on the DOA estimation method [22] for stability analysis without systematic design, the estimated DOA is $\{\Delta x \in \mathbb{R}^{13} \mid -1.02x_e \leq \Delta x \leq 0.26x_e\}$ with a given $\lambda = 2$. The estimated DOA does not encompass the L/HVRT boundary, potentially jeopardizing system stability. Engineers may need to use additional methods like the sensitivity-based approach [43] to ensure stability. In contrast, the systematic design ensures a feasible range of λ for set-covering, alleviating the need for engineers to engage in extra parameter tuning for stability guarantee.

4) Discussion: Not all droop gains outside $\mathcal{K}'$ will lead to instability. This is because the quadratic Lyapunov function represents a sufficient condition for transient stability, and (15)-(16) only quantifies a subset of the actual DOA. Furthermore, the proposed approach focuses on ensuring that the designated operational range is a subset of the actual DOA. The control objective does not include transient performance, which may vary as control parameters change within the feasible region obtained. However, transient performance could be a design objective, as discussed in [44], [45]. This systematic design can complement those methods to guarantee stability.

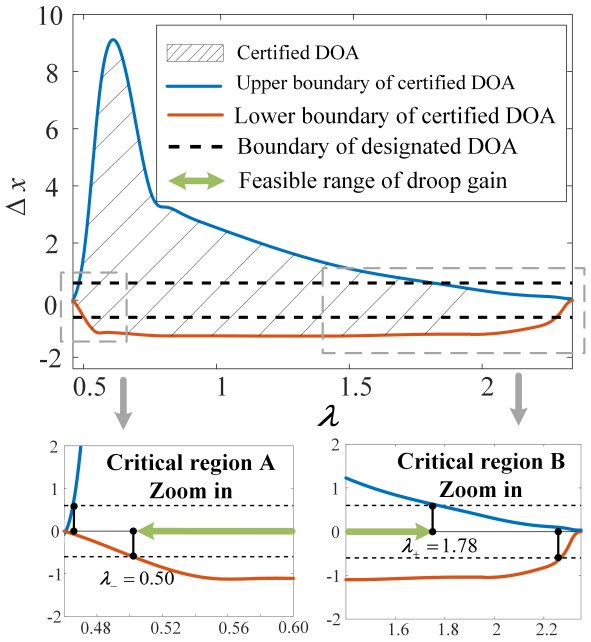

Fig. 6. Visualized systematic droop controller design results for single inverter system based on simplified IBR model.

The proposed method can also include fault recovery capability design by incorporating the initial post-fault state in the designated DOA. The state can be determined by considering different types of faults and a defined time threshold for fault clearing. If the initial post-fault state falls within the designated DOA, the microgrid can recover from faults without any stability concerns when equipped with the designed controller.

B. Modified Banshee Microgrid

This subsection further verifies the proposed method in the modified Banshee microgrid.

1) System configuration: As shown in Fig. 7, the microgrid used for testing is a modification of the Banshee distribution system [46], [47]. The modification involves keeping feeder 1 and integrating renewable energy and energy storage devices, resulting in a self-sufficient system that operates in islanded mode with switch 100 off. Three GFM inverters are connected to Bus 105, Bus 103, and Bus 102, each with distinct rated capacities of 1500 kVA, 3000 kVA, and 4500 kVA. These rated capacities serve as a reference for initiating the droop gain vector.

2) Systematic droop controller design: The objective is to find the droop gain set that can ensure stability and DOA under L/HVRT conditions, similar to the single-inverter system design. Therefore, assume $K = [k_{dv,1}, k_{df,1}, k_{dv,2}, k_{df2}, k_{dv,3}, k_{df,3}]$.

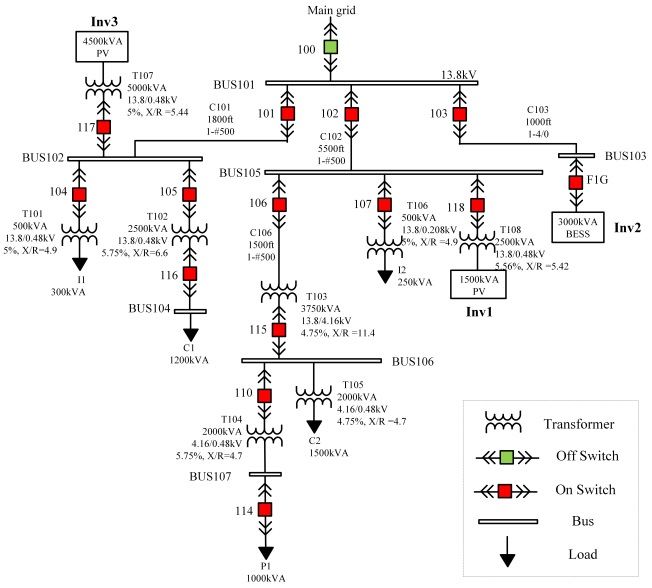

Fig. 7. Single-line diagram of modified Banshee microgrid [46].

Engineering practice typically tunes droop gains of GFM inverters in proportion to their rated capacity to share microgrid loads. Specifically, $k_{dv,1} : k_{dv,2} : k_{dv,3} = k_{df,1} : k_{df,2} : k_{df,3} = S_1 : S_2 : S_3$. Assume $K_0 = [0.017, 0.0033, 0.035, 0.0067, 0.05, 0.01]$, then λ_- and λ_+ are solved as 0.028 and 1.513 based on *Algorithm 1*, and the candidate droop gain set is obtained as $\mathcal{K}' = \{K \in \mathbb{R}^6 \mid K = \lambda K_0, 0.028 \leq \lambda \leq 1.513\}$.

3) Numerical Verification: The dynamic performance of inverters under the systematic design is verified by randomly sampling droop gain vectors from $\mathcal{K}'$. Results show that all state variables can converge to equilibrium. For instance, with $\lambda = 1$ and $K = [0.017, 0.0033, 0.035, 0.0067, 0.05, 0.01]$, the three-dimensional voltage trajectories of the three GMF inverters are shown in Fig. 8 when initialized from the varying L/HVRT boundary. Eight initial points starting from the cube's vertices converge to equilibrium. The transient trajectories of some other key state variables are further shown in Fig. 9 when initialized from $[v_{d1}, v_{d2}, v_{d3}] = [0.6, 0.6, 0.6]$. All state variables converge around 0.15 s, indicating the correct methodology. However, the state variables diverge if λ is set to 2, as depicted in Fig. 10.

4) Comparison: Referring to the comparison conducted in the single inverter system, the candidate droop gain set of the modified Banshee microgrid is obtained as $\mathcal{K}' = \{K \in \mathbb{R}^6 \mid K = \lambda K_0, 0.48 \leq \lambda \leq 1.47\}$ using a simplified IBR model. The design results are more conservative than those obtained from the full-scale EMT model. If solely relying on the DOA estimation method for stability analysis without systematic design, the estimated DOA is $\{\Delta x \in \mathbb{R}^{13} \mid -0.98x_e \leq \Delta x \leq 0.12x_e\}$ given $\lambda = 1.4$. Such a design can potentially lead to operational risks because the estimated DOA fails to cover the L/HVRT range, necessitating extensive parameter tuning to ensure stability. These adjustments are known to be time-intensive, thus highlighting the superiority of the proposed method.

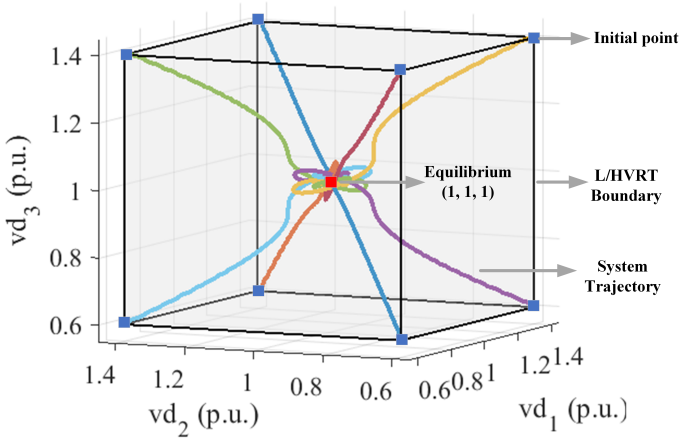

Fig. 8. Three-dimensional voltage trajectories with varying initial conditions.

C. Power HIL Verification for the modified Banshee microgrid controller design

The systematic controller design for the modified Banshee microgrid is further demonstrated through power HIL experiments. A hardware test-bed (HTB) platform is developed by the Center for Ultrawide Area Resilient Electric Transmission Networks (CURENT) at the University of Tennessee [48], [49]. This platform allows for replicating power grids by programming IBRs to mimic grid components. Fig. 11 shows the diagram of HTB, where Fig. 11a shows the hardware system overview and Fig. 11b shows the communication structure. The connection line is created using actual inductance, which also includes the transformer's impedance. The rest of the components in Fig. 7 are all emulated by IBRs. For a more comprehensive understanding of the measurement, control, and communication architecture, please refer to Section III in [48].

Referring to the numerical verification, droop gains are randomly sampled from the obtained candidate set and tested in HTB under LVRT conditions. Due to the capability constraints of HTB and its built-in protection schemes, it is difficult to emulate LVRT conditions for all three inverters at the same time. Therefore, only inverter 1 is subjected to LVRT conditions by injecting a large external inductive reactive power into BUS 106.

The power HIL test results are shown in Fig. 12. Fig. 12a depicts IBRs with droop gains assigned at $\lambda = \lambda_-$, where the terminal voltage of inverter 1 drops to the LVRT boundary around 1.7 s due to inductive reactive power injection. The voltage recovers to the nominal value after the disturbance is cleared around 2.2 s. During the disturbance, the system frequency experiences mild deviations. Similarly, Fig. 12a displays the system voltage and frequency when IBRs are assigned droop gains with $\lambda = \lambda_+$. Even with a voltage droop that reaches the LVRT boundary, inverter 1 can continue operating until the disturbance is resolved. Beyond the results displayed in Fig. 12, a few other gains are randomly selected

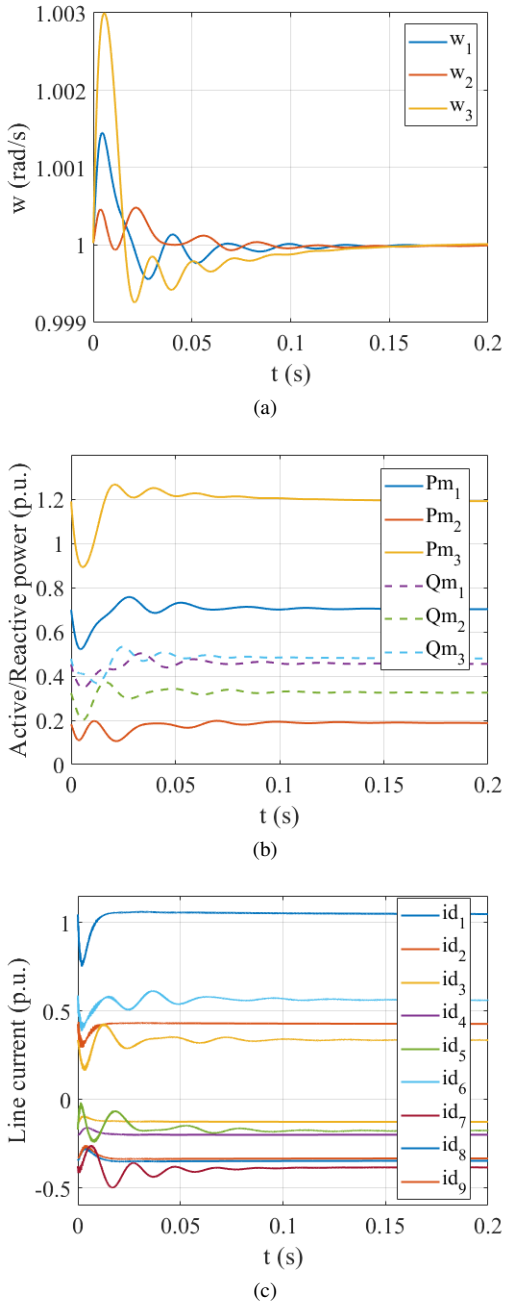

Fig. 9. Transient trajectories of Banshee microgrid (partial) with $\lambda = 1$: (a) Angle frequency; (b) Power output of inverter; (c) Grid line current.

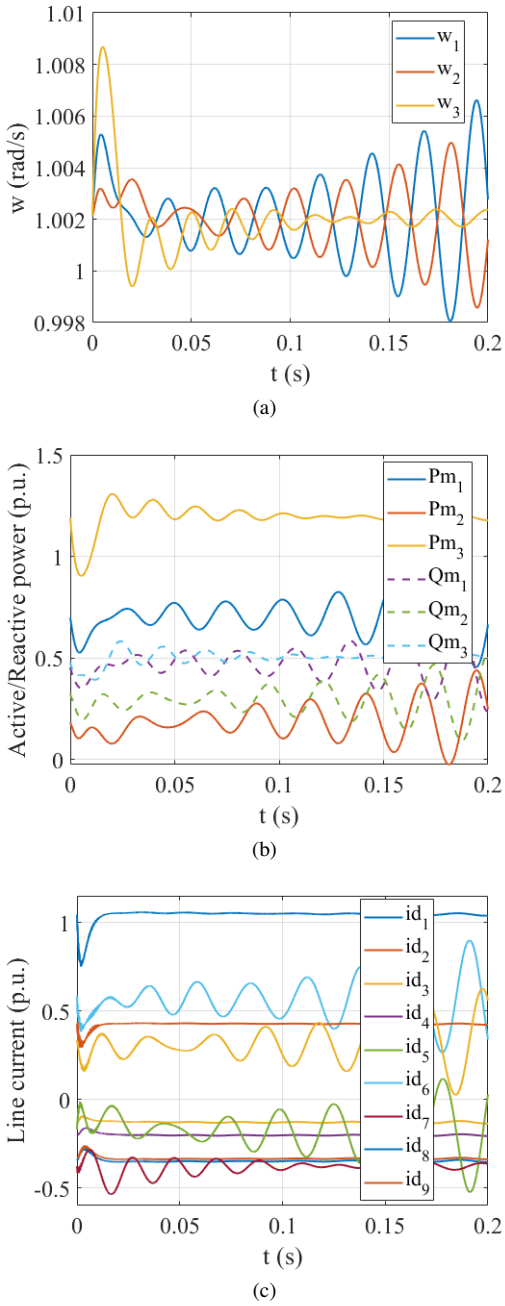

Fig. 10. Transient trajectories of Banshee microgrid (partial) with $\lambda = 2$: (a) Angle frequency; (b) Power output of inverter; (c) Grid line current.

and tested. The system consistently returns to its original equilibrium point after disturbances, proving the effectiveness of the formulated homogeneous-like EMT model and the systematic controller design approach.

In summary, the proposed method can ensure the stability of the modified Banshee microgrid. Based on *Lemma 4*, $\mathcal{K}'$ rigorously guarantees stability and designated DOA. With the design results in mind, some adaptive algorithms that update the droop gains online can work safely and reliably under L/HVRT conditions. This is extremely significant since IBRs are expected to actively provide grid support and enhance microgrid resilience in the event of natural and man-made hazards that could jeopardize the system.

V. Conclusion

This paper proposes a systematic approach for inverter-based microgrids to certify stability and a designated DOA. A nonlinear EMT model is developed to accurately capture the fast dynamics of grid components, which is then transformed into a homogeneous-like system to facilitate the analytical stability derivation. The nonlinear terms are treated as superimposed parameter uncertainties and bounded within

(a)

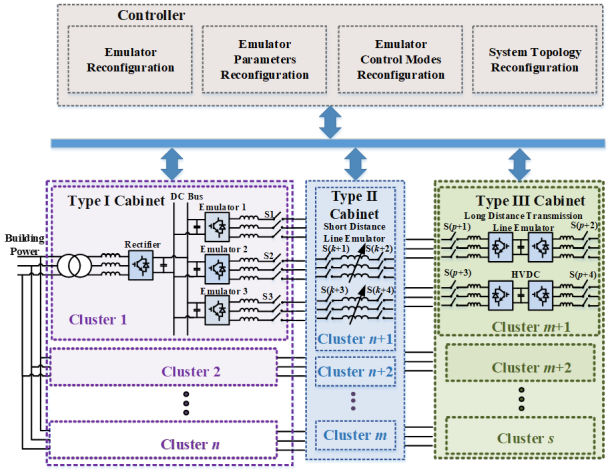

(b)

Fig. 11. Diagram of HTB: (a) hardware system overview; (b) communication structure.

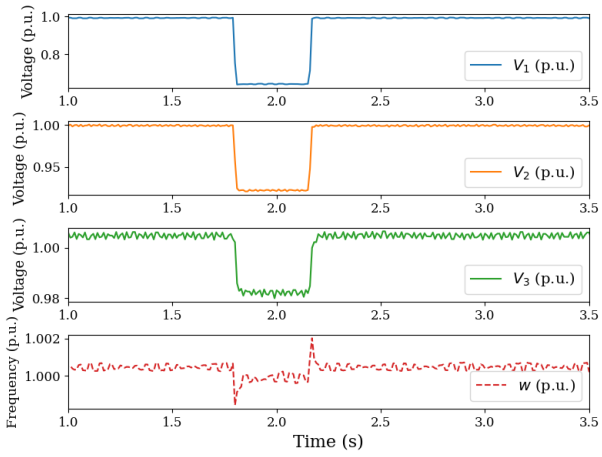

(a)

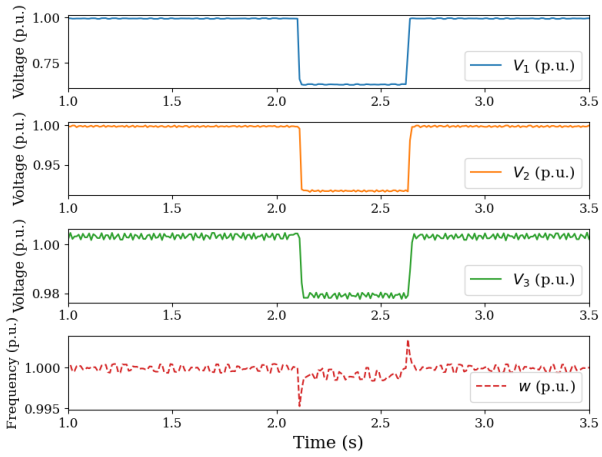

(b)

Fig. 12. Power HIL test results: (a) $\lambda = 0.028$, the lower boundary of $\mathcal{K}'$; (b) $\lambda = 1.153$, the upper boundary of $\mathcal{K}'$.

a specific range to derive the stability criteria. Utilizing the stability criteria, a systematic controller design approach is further developed to identify the candidate control parameter set that ensures stability and DOA whenever in normal or emergency conditions. The proposed methodology shows great flexibility and can be integrated into some adaptive approaches and physic-informed data-driven approaches for stability and performance guarantee. In the future, detailed integration strategies will be investigated to harness the full potential of the proposed systematic approach.

ACKNOWLEDGMENT

The authors would like to thank the financial support from US DOD and DOE. UTK's work is supported in part by the US DOD ESTCP program under grant number EW20-5331, and ANL's work is supported in part by the US DOE Advanced Grid Modeling Program under grant number DE-OE0000875.

REFERENCES

[1] B. She, F. Li, H. Cui, J. Zhang, and R. Bo, "Fusion of microgrid control with model-free reinforcement learning: Review and vision," *IEEE Transactions on Smart Grid*, 2022.

[2] A. Vasilakis, I. Zafeiratou, D. T. Lagos, and N. D. Hatziargyriou, "The evolution of research in microgrids control," *IEEE Open Access Journal of Power and Energy*, vol. 7, pp. 331–343, 2020.

[3] L. Wang, Y. Qin, Z. Tang, and P. Zhang, "Software-defined microgrid control: The genesis of decoupled cyber-physical microgrids," *IEEE Open Access Journal of Power and Energy*, vol. 7, pp. 173–182, 2020.

[4] X. Li, P. Lin, Y. Tang, and K. Wang, "Stability design of single-loop voltage control with enhanced dynamic for voltage-source converters with a low lc-resonant-frequency," *IEEE Transactions on Power Electronics*, vol. 33, no. 11, pp. 9937–9951, 2018.

[5] B. She, F. Li, H. Cui, J. Wang, Q. Zhang, and R. Bo, "Virtual inertia scheduling (VIS) for real-time economic dispatch of ibrs-penetrated power systems," *IEEE Transactions on Sustainable Energy*, 2023.

[6] P. Lin, C. Zhang, J. Wang, C. Jin, and P. Wang, "On autonomous large-signal stabilization for islanded multibus dc microgrids: A uniform non-smooth control scheme," *IEEE Transactions on Industrial Electronics*, vol. 67, no. 6, pp. 4600–4612, 2019.

[7] U. Markovic, O. Stanojev, P. Aristidou, E. Vrettos, D. Callaway, and G. Hug, "Understanding small-signal stability of low-inertia systems," *IEEE Transactions on Power Systems*, vol. 36, no. 5, pp. 3997–4017, 2021.

[8] A. Lasheen, M. E. Ammar, H. H. Zeineldin, A. Al-Durra, M. F. Shaaban, and E. El-Saadany, "Assessing the impact of reactive power droop on inverter based microgrid stability," *IEEE Transactions on Energy Conversion*, vol. 36, no. 3, pp. 2380–2392, 2021.

[9] X. Guo, Z. Lu, B. Wang, X. Sun, L. Wang, and J. M. Guerrero, "Dynamic phasors-based modeling and stability analysis of droop-controlled inverters for microgrid applications," *IEEE Transactions on Smart Grid*, vol. 5, no. 6, pp. 2980–2987, 2014.

[10] A. A. A. Radwan and Y. A.-R. I. Mohamed, "Modeling, analysis, and stabilization of converter-fed ac microgrids with high penetration of converter-interfaced loads," *IEEE Transactions on Smart Grid*, vol. 3,

no. 3, pp. 1213–1225, 2012.

[11] A. F. El-Hamalawy, M. E. Ammar, H. F. Sindi, M. F. Shaaban, and H. H. Zeineldin, "A subspace identification technique for real-time stability assessment of droop based microgrids," *IEEE Transactions on Power Systems*, vol. 37, no. 4, pp. 2731–2743, 2021.

[12] M. N. Hussain, R. Mishra, and V. Agarwal, "A self-switched virtual impedance based stabilization method for a droop controlled dc microgrid with constant power loads and input load filters," in *2016 IEEE International Conference on Power Electronics, Drives and Energy Systems (PEDES)*. IEEE, 2016, pp. 1–6.

[13] R. Turner, S. Walton, and R. Duke, "A case study on the application of the nyquist stability criterion as applied to interconnected loads and sources on grids," *IEEE Transactions on Industrial Electronics*, vol. 60, no. 7, pp. 2740–2749, 2012.

[14] Y. Yan, D. Shi, D. Bian, B. Huang, Z. Yi, and Z. Wang, "Small-signal stability analysis and performance evaluation of microgrids under distributed control," *IEEE Transactions on Smart Grid*, vol. 10, no. 5, pp. 4848–4858, 2018.

[15] P. Pareek and H. D. Nguyen, "A convexification approach for small-signal stability constrained optimal power flow," *IEEE Transactions on Control of Network Systems*, vol. 8, no. 4, pp. 1930–1941, 2021.

[16] M. Kabalan, P. Singh, and D. Niebur, "Large signal lyapunov-based stability studies in microgrids: A review," *IEEE Transactions on Smart Grid*, vol. 8, no. 5, pp. 2287–2295, 2016.

[17] ——, "A design and optimization tool for inverter-based microgrids using large-signal nonlinear analysis," *IEEE Transactions on Smart Grid*, vol. 10, no. 4, pp. 4566–4576, 2018.

[18] D. Karimipour and F. R. Salmasi, "Stability analysis of ac microgrids with constant power loads based on popov's absolute stability criterion," *IEEE Transactions on Circuits and Systems II: Express Briefs*, vol. 62, no. 7, pp. 696–700, 2015.

[19] E. Alves, G. Bergna-Diaz, D. Brandao, and E. Tedeschi, "Sufficient conditions for robust frequency stability of ac power systems," *IEEE Transactions on Power Systems*, vol. 36, no. 3, pp. 2684–2692, 2020.

[20] Y. Tang, Z. Tian, X. Zha, X. Li, M. Huang, and J. Sun, "An improved equal area criterion for transient stability analysis of converter-based microgrid considering nonlinear damping effect," *IEEE Transactions on Power Electronics*, vol. 37, no. 9, pp. 11 272–11 284, 2022.

[21] M. Kabalan, P. Singh, and D. Niebur, "Large signal stability analysis of a dc/ac droop controlled inverter connected to an infinite bus," in *2015 North American Power Symposium (NAPS)*. IEEE, 2015, pp. 1–6.

[22] Z. Zhang, R. Schuerhuber, L. Fickert, K. Friedl, G. Chen, and Y. Zhang, "Domain of attraction's estimation for grid connected converters with phase-locked loop," *IEEE Transactions on Power Systems*, vol. 37, no. 2, pp. 1351–1362, 2021.

[23] X. Fu, J. Sun, M. Huang, Z. Tian, H. Yan, H. H.-C. Iu, P. Hu, and X. Zha, "Large-signal stability of grid-forming and grid-following controls in voltage source converter: A comparative study," *IEEE Transactions on Power Electronics*, vol. 36, no. 7, pp. 7832–7840, 2020.

[24] K. D. Smith, S. Jafarpour, and F. Bullo, "Transient stability of droop-controlled inverter networks with operating constraints," *IEEE Transactions on Automatic Control*, vol. 67, no. 2, pp. 633–645, 2021.

[25] Y. Du, Y. Men, L. Ding, and X. Lu, "Large-signal stability analysis for inverter-based dynamic microgrids reconfiguration," *IEEE Transactions on Smart Grid*, 2021.

[26] T. Huang, S. Gao, and L. Xie, "A neural lyapunov approach to transient stability assessment of power electronics-interfaced networked microgrids," *IEEE Transactions on Smart Grid*, vol. 13, no. 1, pp. 106–118, 2021.

[27] C. A. Aragon, R. Guzman, L. G. de Vicuña, J. Miret, and M. Castilla, "Constrained predictive control based on a large-signal model for a three-phase inverter connected to a microgrid," *IEEE Transactions on Industrial Electronics*, vol. 69, no. 7, pp. 6497–6507, 2021.

[28] J. Chen and J. Chen, "Stability analysis and parameters optimization of islanded microgrid with both ideal and dynamic constant power loads," *IEEE Transactions on Industrial Electronics*, vol. 65, no. 4, pp. 3263–3274, 2017.

[29] W. Cui and B. Zhang, "Lyapunov-regularized reinforcement learning for power system transient stability," *IEEE Control Systems Letters*, vol. 6, pp. 974–979, 2021.

[30] M. Kabalan, P. Singh, and D. Niebur, "Nonlinear lyapunov stability analysis of seven models of a dc/ac droop controlled inverter connected to an infinite bus," *IEEE Transactions on Smart Grid*, vol. 10, no. 1, pp. 772–781, 2017.

[31] T. Demiray, "Simulation of power system dynamics using dynamic phasor models," Ph.D. dissertation, ETH Zurich, 2008.

[32] F. D. Mohammadi, H. K. Vanashi, and A. Feliachi, "State-space modeling, analysis, and distributed secondary frequency control of isolated microgrids," *IEEE Transactions on Energy Conversion*, vol. 33, no. 1, pp. 155–165, 2017.

[33] S. Wiggins, S. Wiggins, and M. Golubitsky, *Introduction to applied nonlinear dynamical systems and chaos*. Springer, 2003, vol. 2, no. 3.

[34] K. Mahmoud, P. H. Divshali, P. Peltoniemi, and M. Lehtonen, "Promising grid-forming vsc control schemes towards sustainable power systems: Comprehensive review and perspectives," *IEEE Access*, 2022.

[35] Z. Zhang, X. You, H. Ma, K. Zhao, and N. Zhou, "Research on application of low voltage ride through technology of auxiliary equipment inverter of thermal power plant in power grid," in *2021 6th Asia Conference on Power and Electrical Engineering (ACPEE)*. IEEE, 2021, pp. 1446–1450.

[36] J. Liu, Y. Zhang, A. J. Conejo, and F. Qiu, "Ensuring transient stability with guaranteed region of attraction in dc microgrids," *IEEE Transactions on Power Systems*, 2022.

[37] A. Ben-Tal, L. El Ghaoui, and A. Nemirovski, *Robust optimization*. Princeton university press, 2009, vol. 28.

[38] S. Boyd, S. P. Boyd, and L. Vandenberghe, *Convex optimization*. Cambridge University Press, 2004.

[39] M. Farrokhabadi, C. A. Cañizares, J. W. Simpson-Porco, E. Nasr, L. Fan, P. A. Mendoza-Araya, R. Tonkoski, U. Tamrakar, N. Hatziargyriou, D. Lagos *et al.*, "Microgrid stability definitions, analysis, and examples," *IEEE Transactions on Power Systems*, vol. 35, no. 1, pp. 13–29, 2019.

[40] IEEE, *IEEE Standard for Interconnection and Interoperability of Distributed Energy Resources with Associated Electric Power Systems Interfaces*, Std., 2018. [Online]. Available: https://ieeexplore.ieee.org/document/8332112

[41] X. Wang, L. Ding, Z. Ma, R. Azizipanah-Abarghooee, and V. Terzija, "Perturbation-based sensitivity analysis of slow coherency with variable power system inertia," *IEEE Transactions on Power Systems*, vol. 36, no. 2, pp. 1121–1129, 2020.

[42] D. Brahma and N. Senroy, "Estimation of dynamic grid flexibility using matrix perturbation theory," *IEEE Transactions on Power Systems*, vol. 37, no. 3, pp. 2491–2494, 2022.

[43] H. Zheng, X. Yuan, J. Cai, P. Sun, and L. Zhou, "Large-signal stability analysis of dc side of vsc-hvdc system based on estimation of domain of attraction," *IEEE Transactions on Power Systems*, vol. 37, no. 5, pp. 3630–3641, 2022.

[44] S. Deng, L. Chen, X. Lu, T. Zheng, and S. Mei, "Distributed finite-time secondary frequency control of islanded microgrids with enhanced operational flexibility," *IEEE Transactions on Energy Conversion*, vol. 36, no. 3, pp. 1733–1742, 2021.

[45] R. Lu, J. Wang, and Z. Wang, "Distributed observer-based finite-time control of ac microgrid under attack," *IEEE Transactions on Smart Grid*, vol. 12, no. 1, pp. 157–168, 2020.

[46] R. Salcedo, E. Corbett, C. Smith, E. Limpaecher, R. Rekha, J. Nowocin, G. Lauss, E. Fonkwe, M. Almeida, P. Gartner *et al.*, "Banshee distribution network benchmark and prototyping platform for hardware-in-the-loop integration of microgrid and device controllers," *The Journal of Engineering*, vol. 2019, no. 8, pp. 5365–5373, 2019.

[47] B. She, F. Li, H. Cui, J. Wang, L. Min, O. Oboreh-Snapps, and R. Bo, "Decentralized and coordinated V-f control for islanded microgrids considering der inadequacy and demand control," *IEEE Transactions on Energy Conversion*, pp. 1–13, 2023.

[48] S. Zhang, B. Liu, S. Zheng, Y. Ma, F. Wang, and L. M. Tolbert, "Development of a converter-based transmission line emulator with three-phase short-circuit fault emulation capability," *IEEE Transactions on Power Electronics*, vol. 33, no. 12, pp. 10 215–10 228, 2018.

[49] L. M. Tolbert, F. Wang, K. Tomsovic, K. Sun, J. Wang, Y. Ma, and Y. Liu, "Reconfigurable real-time power grid emulator for systems with high penetration of renewables," *IEEE Open Access Journal of Power and Energy*, vol. 7, pp. 489–500, 2020.

Buxin She (Student Member, IEEE) is presently a Ph.D. student in the Department of Electrical Engineering and Computer Science at The University of Tennessee, Knoxville. He received his B.S.E.E. and M.S.E.E. degrees both from Tianjin University, Tianjin, China in 2017 and 2019, respectively. He was an outstanding reviewer of MPCE and IEEE OAJPE. He is a student guest editor of IET-RPG. His research interests include microgrid operation and control, machine learning in power systems, distribution system plan, and power grid resilience.

Jianzhe Liu (Member, IEEE) is an Energy Systems Scientist at Argonne National Laboratory and holds a joint-appointment at the University of Chicago. He received the B.E. degree in electrical engineering from Huazhong University of Science and Technology, China, in 2012, and the Ph.D. degree in electrical and computer engineering from The Ohio State University, U.S.A., in 2017. His research interests include the optimization and control of power electronics enabled energy systems.

Feng Qiu (Senior Member, IEEE) received the Ph.D. degree in optimization from the School of Industrial and Systems Engineering, Georgia Institute of Technology, Atlanta, GA, USA, in 2013., He is a Principal Computational Scientist with the Energy Systems Division, Argonne National Laboratory, Argonne, IL, USA. His current research interests include optimization in power system operations, electricity markets, and power grid resilience.

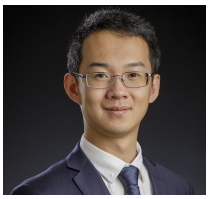

Hantao Cui (Senior Member, IEEE) received the B.S. and M.S. degrees from Southeast University, China in 2011 and 2013, and the Ph.D. degree from the University of Tennessee, Knoxville in 2018, all in electrical engineering. He is currently an Assistant Professor with the School of Electrical and Computer Engineering, Oklahoma State University. His research interests include power system modeling, simulation, and high-performance computing.

Nattapat Praisuwanna (Student Member, IEEE) is a Ph.D. student in Electrical Engineering at the University of Tennessee. He received both B.S. and M.S. degrees in electrical engineering from King Mongkut's Institute of Technology Ladkrabang, Bangkok, Thailand in 2009 and 2011, respectively. His research interests include power converters, renewable energy application, and renewable energy.

Jingxin Wang (Member, IEEE) is a research associate with the Department of Electrical Engineering and Computer Science, The University of Tennessee, Knoxville. He received Ph.D. degree in power electronics and electrical drives from Shanghai Jiao Tong University in 2011. His research interests include high-performance motor control, modular multilevel converter, power flow control, and renewable energy.

Leon M. Tolbert (Fellow, IEEE) received the bachelor's, M.S., and Ph.D. degrees in electrical engineering from the Georgia Institute of Technology, Atlanta, GA, USA, in 1989, 1991, and 1999, respectively. From 1991 to 1999, he was with the Oak Ridge National Laboratory, Oak Ridge, TN, USA. In 1999, he was appointed as an Assistant Professor with the Department of Electrical and Computer Engineering, The University of Tennessee, Knoxville, TN, USA, where he is currently the Min H. Kao Professor with the Min H. Kao Department of Electrical Engineering and Computer Science. He is also a Founding Member of the NSF/DOE Engineering Research Center for Ultra-Wide-Area Resilient Electric Energy Transmission Networks (CURENT). Dr. Tolbert is a Registered Professional Engineer in the State of Tennessee. He was a recipient of the 2001 IEEE Industry Applications Society Outstanding Young Member Award and eight prize paper awards from the IEEE Industry Applications Society and IEEE Power Electronics Society. He was an Associate Editor of the IEEE Transaction on Power Electronics, from 2007 to 2013. He was the Paper Review Chair for the Industry Power Converter Committee of the IEEE Industry Applications Society, from 2014 to 2017. He is the deputy editor-in-chief of the IEEE Power Electronics Magazine and the Publications Chair for the IEEE Industry Applications Society.

Fangxing Li (Fellow, IEEE) is also known as Fran Li. He received the B.S.E.E. and M.S.E.E. degrees from Southeast University, Nanjing, China, in 1994 and 1997, respectively, and the Ph.D. degree from Virginia Tech, Blacksburg, VA, USA, in 2001. Currently, he is the James W. McConnell Professor in electrical engineering at the University of Tennessee, Knoxville (UTK), TN, USA. He is also a Founding Member of CURENT, an NSF/DOE Engineering Research Center headquartered at UTK, and serves as the UTK Campus Director of CURENT. His research interests include resilience, artificial intelligence in power, demand response, distributed generation and microgrid, and electricity markets. From 2020 to 2021, he served as the Chair of IEEE PES Power System Operation, Planning, and Economics (PSOPE) Committee. He has been serving as the Chair of IEEE WG on Machine Learning for Power Systems since 2019 and the Editor-In-Chief of IEEE Open Access Journal of Power and Energy (OAJPE) since 2020. Prof. Li has received numerous awards and honors including R&D 100 Award in 2020, IEEE PES Technical Committee Prize Paper award in 2019, 5 best or prize paper awards at international journals, and 7 best papers/posters at international conferences.